

Journal of Materials Chemistry A

Accepted Manuscript



This is an *Accepted Manuscript*, which has been through the Royal Society of Chemistry peer review process and has been accepted for publication.

Accepted Manuscripts are published online shortly after acceptance, before technical editing, formatting and proof reading. Using this free service, authors can make their results available to the community, in citable form, before we publish the edited article. We will replace this *Accepted Manuscript* with the edited and formatted *Advance Article* as soon as it is available.

You can find more information about *Accepted Manuscripts* in the [Information for Authors](#).

Please note that technical editing may introduce minor changes to the text and/or graphics, which may alter content. The journal's standard [Terms & Conditions](#) and the [Ethical guidelines](#) still apply. In no event shall the Royal Society of Chemistry be held responsible for any errors or omissions in this *Accepted Manuscript* or any consequences arising from the use of any information it contains.

CuInSe₂ and CuInSe₂-ZnS based High Efficiency “Green” Quantum Dot Sensitized Solar Cells

Wenjie Li, Zhenxiao Pan, and Xinhua Zhong*

Key Laboratory for Advanced Materials, Institute of Applied Chemistry, East China University of Science and Technology, Shanghai 200237, China

Email: zhongxh@ecust.edu.cn

ABSTRACT

CuInSe₂ (CISE) based quantum dots (QDs), are perceived to be a promising alternative to those cadmium or lead chalcogenide based QDs in serving as light-harvesting sensitizer materials in quantum dot sensitized solar cells (QDSCs) due to their near-infrared (NIR) absorbing capacity and low toxicity. Herein, we have synthesized high quality CISE QDs via the organic phase high temperature route, and then alloying with ZnS to form the CISE-ZnS QDs with higher chemical stability and superior optoelectronic properties. The obtained “green” CISE and CISE-ZnS QD sensitizers were immobilized onto TiO₂ film electrodes with high loading amount through the linker molecule assisted postsynthesis assembly approach with use of MPA-capped water-soluble QDs. Hindered charge recombination in the built CISE-ZnS QD based solar cells in comparison with reference CISE cells has been confirmed by impedance spectroscopy, as well as transient photovoltage decay measurements. With combination of high QD loading and passivated trap-state defects, the resulting regenerative sandwich CISE-ZnS QD based champion solar cells exhibit an efficiency of 6.79% ($J_{sc} = 22.61 \text{ mA/cm}^2$, $V_{oc} = 0.583 \text{ V}$, $FF = 0.515$) under AM 1.5G full one sun irradiation. The obtained efficiency is among the best performances for liquid-junction QDSCs and also demonstrates the comparable photovoltaic performance of “green” CISE based QDs to the toxic cadmium and lead chalcogenide QDs.

1. Introduction

With the increasingly urgent need for clean energy, unremitting endeavor is made on the direct conversion of solar energy into electricity through photovoltaic (PV) devices.¹⁻³ Among these, quantum dot-sensitized solar cells (QDSCs) have emerged as a promising candidate in the third generation solar cells,^{4,5} with the potential of theoretical power conversion efficiency (PCE) surpassing Shockley–Queisser limit of 32% due to the possibility of extraction of hot electrons and multiple exciton generation (MEG).^{6,7} The ongoing development of QDSCs was addressed by a series of QD sensitizers, including the conventional Cd-based (CdS, CdSe, CdSe_xS_{1-x}, CdSe_xTe_{1-x}) and Pb-based (PbS, PbSe) QDs, among which PCEs were improved from less than 1% to 6-7%.⁸⁻¹⁴ These Cd, Pb-containing QDs based solar cells indeed exhibit excellent photo- and chemical stability, and high PCEs, but the intrinsic high toxicity of Cd or Pb still restricts the commercial application of QDSCs. Hence, exploring high quality “green” QDs sensitizers without carcinogenic heavy metal elements is in great demand.

Pioneering work has been accomplished to explore the low-toxic I-III-VI₂ alloyed QDs for application in PV devices because of its unique properties of high absorption coefficient ($\sim 10^5 \text{ cm}^{-1}$) and relative narrow band gap.¹⁵⁻¹⁸ These I-III-VI₂ compounds were deemed as better light-harvesting sensitizer materials to take place of II-VI QDs. For example, the PCE of CuInS₂ based QDSCs has been improved steadily to the level comparable to those of toxic cadmium chalcogenides based QDSC.¹⁹⁻²⁴ More importantly, in the near recently, an unprecedented new PCE record of 7.04% has been obtained from CuInS₂ based QDSC by Zhong and coworkers.²⁵ However, CuInSe₂ (CISe) QDs, compared to CuInS₂ (CIS), is considered as a more promising material with larger exciton Bohr radius ($\sim 10.6 \text{ nm}$) and narrower band gap (1.04 vs. 1.5 eV), which can broaden the light-absorbing range to near-infrared (NIR) region.^{26,27} This is the reason why CuInSe_{1-x}S_x QDs were developed in Klimov’s work and outstanding performances were obtained in the resultant CuInSe_{1-x}S_x QDSCs with remarkably improved stability and PCE (up to 5.5%).^{28,29} Furthermore, a variety of synthetic approaches for CISe QDs have been developed.³⁰⁻³⁴ This provides versatile choices for its application in PV devices as light-absorber. Korgel et al. reported a modified synthetic approach for CISe QDs with the use of secondary phosphine as capping ligand.³⁵ These promising findings about the I-III-VI₂ QDSCs have triggered considerable attention in the construction of high efficiency “green” QDSCs.

Recent progress has emphasized the importance of band gap tailoring and stability improvement in the I-III-VI₂ QDs for their photovoltaic applications.²⁹ Generally, broader light harvesting range is achieved with the use of larger sized QDs. However, large sized QD brings forward the difficulty in penetrating into mesoporous oxide film, and in electron injection from QD sensitizer into TiO₂, resulting in low PCEs.²⁹ Alloying CISE with other wider band gap materials is a favorable approach to tune the optoelectronic properties and improve the stability of the resultant QDs, as in the cases of CuInSe_xS_{1-x},²⁹ (CIS)_{1-x}-(ZnS)_x,³⁶ and (CISE)_{1-x}-(ZnSe)_x QDs³⁷. In addition, this alloying process could benefit the electron injection from the band gap tailoring as well as protect and passivate the surface, and therefore outperforms the approach of core-shell structure in serving as light-harvesting materials in QDSCs.^{38,39} In this work, high-quality NIR absorption (CISE)_{1-x}-(ZnS)_x QDs were prepared via the alloying process of CISE QDs with ZnS constituent, followed by a ligand exchange process to obtain water-soluble CISE-ZnS QDs capped by a bifunctional molecule, mercaptopropionic acid (MPA). The MPA-capped QDs were tethered on TiO₂ film electrode via a self-assembling process. With the combination of high loading of QD sensitizer and intrinsic superior optoelectronic properties (broad light-harvesting range, and high chemical stability *etc.*) of the adopted CISE-ZnS alloyed QD sensitizer, the resulting QDSCs exhibit a best performing PCE of 6.79% under full 1 sun illumination, which is among the best performances for liquid-junction QDSCs, and also demonstrates the comparable photovoltaic performance of “green” CISE-based QDs to the toxic cadmium and lead chalcogenide QDs.

2. Experimental section

Materials. Indium acetate ($\text{In}(\text{OAc})_3$, 99.99%), zinc acetate ($\text{Zn}(\text{OAc})_2$, 99.99%), sulfur powder (99.99%), selenium powder (200 mesh, 99.99%), oleylamine (OAm, 97%) were purchased from Aldrich. Copper iodide (CuI , 99.998%), 3-mercaptopropionic acid (MPA, 97%) were received from Alfa Aesar, and diphenylphosphine (DPP, 98%) from J&K. All chemicals were used as received without further processing.

Synthesis of CISE and CISE-ZnS QDs. For a typical synthesis of CISE QDs from a modified literature approach,³⁵ CuI (19.0 mg, 0.1 mmol) and $\text{In}(\text{OAc})_3$ (29.2 mg, 0.1 mmol) were mixed with 4 mL OAm in a flask. The reaction mixture was degassed and then heated to 180°C under argon flow. Then a Se-DPP stock solution (obtained by dissolve 19.7 mg (0.25 mmol) selenium powder in 1 mL DPP) was injected into the reaction mixture and stayed at this temperature for 10 min. Afterwards the heating was removed and the reaction mixture was cooled at room temperature and dispersed in toluene. Further purification was carried out by precipitation and centrifugation procedure with the use of acetone. $\text{CISE}_{0.8}\text{-ZnS}_{0.2}$ NCs were obtained similarly, by loading CuI (19.0 mg, 0.1 mmol), $\text{In}(\text{OAc})_3$ (29.2 mg, 0.1 mmol) and $\text{Zn}(\text{OAc})_2$ (11.0 mg, 0.05 mmol) into the flask together with 4 mL of OAm, followed by the injection of Se and S precursors mixture stock solution (obtained by dissolving 0.25 mmol selenium powder and 0.05 mmol sulfur powder in 1 mL DPP) into the reaction mixture at 180°C. $\text{CISE}_{0.7}\text{-ZnS}_{0.3}$ NCs were prepared by increasing the amount of $\text{Zn}(\text{OAc})_2$ (0.1 mmol) and sulfur powder (0.1 mmol). The final element ratio is determined by the ICP analysis.

Immobilization of QDs onto TiO_2 Film electrodes and Construction of Solar Cells. TiO_2 mesoporous films ($9.0 \pm 0.5 \mu\text{m}$ transparent layer together with $6.0 \pm 0.5 \mu\text{m}$ light scattering layer) were prepared according to literature method.^{40,41} Ligand exchange procedure was accomplished to make the initial OAm-capped oil-soluble QDs water-soluble with use of a bifunctional capping ligand MPA.^{14,42} The MPA capped water-soluble QDs were attached to the TiO_2 mesoporous film by pipetting the QD aqueous solution onto the film and staying stationary for 2 h. A ZnS barrier layer was overcoated on the sensitized photoanodes by dipping the electrode alternately into 0.1 M $\text{Zn}(\text{OAc})_2$ and 0.1 M Na_2S aqueous solutions for 4 cycles.²⁵ Finally, the QDs-sensitized solar cells were fabricated with a Sandwich configuration by assembling the sensitized TiO_2 photoanode and brass based Cu_2S counter electrode with a binder clip and separated by a 60- μm Scotch spacer. Polysulfide electrolyte solution with composition of 2.0 M Na_2S , 2.0 M S powder and 0.2 M KCl was then injected into the cell device.

Characterization. Transition electron microscopy (TEM) images were acquired on a JEOL JEM-2100 instrument. The absorption and PL emission spectra were recorded on a Shimadzu UV-2600, and a Cary Eclipse (Varian) spectrophotometer, respectively. Powder X-ray diffraction (XRD) was obtained by using a Siemens D5005 X-ray powder diffractometer, equipped with graphite-monochromatized Cu K α radiation ($\lambda=1.5406$ Å). Inductively coupled plasma atomic emission spectroscopy (ICP-AES, Thermo Elemental IRIS 1000) was used to identify the composition information of the QDs. The photovoltaic properties, $J-V$ curves of the QDSCs, were measured by Keithley 2400 source meter equipped with a 150 W AM 1.5 G solar simulator (Oriel, model no. 94022A). Calibration was taken by an NREL standard Si solar cell to set the power of the simulated solar light to 100 mW cm^{-2} . During the measurement, the photoactive area was defined by a shading mask of 0.237 cm^2 . Incident photon-to-current conversion efficiency (IPCE) spectrum was measured by a Keithley 2000 multimeter with illumination of a 300 W tungsten lamp with a Spectral Product DK240 monochromator. Electrochemical impedance spectroscopy (EIS) and open circuit voltage decay (OCVD) measurements were carried out on an electrochemical workstation (Zahner, Zennium). EIS was measured under dark conditions at different forward bias ranged from 0 V to -0.55V, applying a 20 mV AC sinusoidal signal over the constant applied bias with the frequency ranging from 1 MHz to 0.1 Hz. In OCVD measurements, samples were illuminated by a white LED with intensity of 100 mW cm^{-2} , and the dependence of photovoltage on time was recorded after the switch-off of the light.

3. Results and discussion

Optical Properties of CISE and CISE-ZnS QDs. A modified literature approach was adopted for the preparation of high-quality CISE ($3.5 \pm 0.4 \text{ nm}$) and CISE-ZnS ($3.8 \pm 0.3 \text{ nm}$) QDs,³⁵ where the anion precursors with higher reactivity, Se-DPP and S-DPP, were adopted to react with the cation precursors in OAm media at high temperature. Appealing results of the absorption information were obtained, as shown in the absorption spectra (Fig. 1a), with the absorption onset extending to 900 nm, suggesting the superior light-harvesting capacity for application in PV devices. With the variation of the constituent ratio of CISE to ZnS, a series of alloyed (CISE)_{1-x}-(ZnS)_x QDs with tunable band gap were attained and the x values have been verified by ICP analysis, giving a Cu/In/Se composition of 1:1.1:2.1 (near the stoichiometric ratio 1:1:2), and CISE/ZnS composition of 0.8:0.2 and 0.7:0.3 approximately (CISE_{0.8}-ZnS_{0.2} and CISE_{0.7}-ZnS_{0.3}), which differs a little from the nominal elemental ratio

used in the synthesis due to their reactivity discrepancy. XRD results indicate that all the CISE and $(\text{CISE})_{1-x}-(\text{ZnS})_x$ QDs exhibit chalcopyrite structure (JCPDS: No.40-1487) as shown in Fig. 1c. According to the extrapolation of Tauc plot (Fig. 1a inset), bandgap value of the three typical QDs can be determined as 1.37 eV (CISE), 1.41 eV ($\text{CISE}_{0.8}\text{-ZnS}_{0.2}$), and 1.48 eV ($\text{CISE}_{0.7}\text{-ZnS}_{0.3}$).

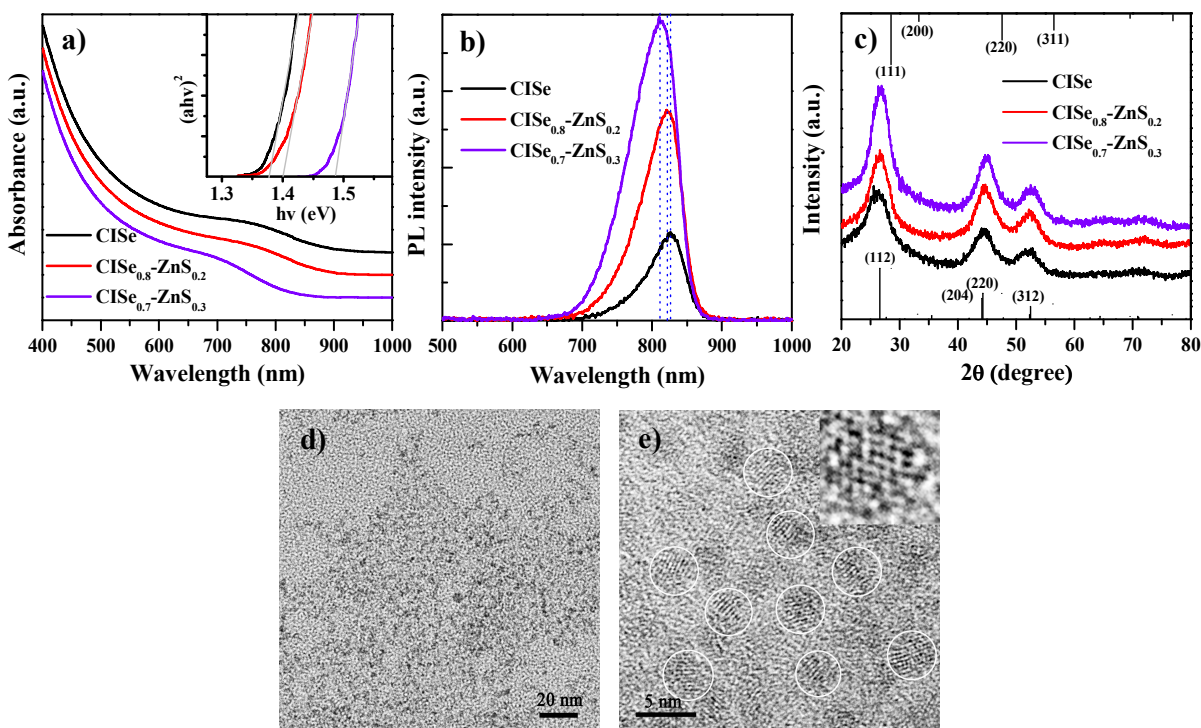


Fig. 1 (a) Normalized UV-vis absorption spectra of CISE, $\text{CISE}_{0.8}\text{-ZnS}_{0.2}$, and $\text{CISE}_{0.7}\text{-ZnS}_{0.3}$ QDs dispersed in toluene, inset diagram showing the Tauc plot for determination of the band gap, (b) PL emission spectra of QD dispersions at same concentration, (c) XRD pattern of the three QDs CISE, $\text{CISE}_{0.8}\text{-ZnS}_{0.2}$, and $\text{CISE}_{0.7}\text{-ZnS}_{0.3}$ with CuInSe_2 (JCPDS: No.40-1487) on the bottom and ZnS (JCPDS: No.05-0566) on the top shown for reference, (d) Wide-field TEM image and (e) HRTEM micrograph of $\text{CISE}_{0.8}\text{-ZnS}_{0.2}$.

Besides band gap tuning, alloying CISE QDs with ZnS constituent also brings forward the reduction of surface defect state and the enhancement of the physiochemical stability of the resulting alloyed QDs. From the optical spectra, we can find that with the incorporation of ZnS constituent into the plain CISE QDs, both of the absorption and PL emission spectra of the resultant $(\text{CISE})_{1-x}-(\text{ZnS})_x$ QDs show a blue-shift. Based on this finding we can consider that the formed $(\text{CISE})_{1-x}-(\text{ZnS})_x$ QDs are in a homogeneous alloy structure, or a gradient alloy structure, with ZnS configuration. Furthermore, as we incorporated ZnS constituent into

the original CISE QDs, the PL intensity of the resultant QDs increased steadily, which can be seen from Fig. 1b. This is the indication of the reduced density of surface defect state. We also observed that the synthesized organic phase (CISE)_{1-x}-(ZnS)_x QDs could be stored for nearly two months without PL intensity quenching, which is much improved in comparison with CISE QDs with PL intensity quenched to half of initial value in one week. This is, on the other hand, proof of the ZnS configuration acting as chemical barrier.

Effective deposition of the QDs sensitizers on TiO₂ mesoporous film. Increasing the loading amount of the QDs sensitizer on the TiO₂ mesoporous film electrode plays a crucial role in boosting PCE of photovoltaic devices. This can be accomplished through an *ex situ* ligand exchange postsynthesis assembly approach, developed by our own group.¹⁴ Our previous work has reported that tethering QDs on TiO₂ film electrode through the *ex situ* ligand exchange route brings forward a high surface coverage (34%) as well as good performance of the resulting QDSCs.^{14,25} Benefiting from the previous experience, this *ex situ* ligand exchange approach was employed to immobilize the CISE or CISE-ZnS QDs on the TiO₂ film electrode, where CISE-ZnS QDs simply refers to CISE_{0.8}-ZnS_{0.2} QDs for convenience. Through the ligand exchange approach, initial OAm-capped oil-soluble QDs were transferred to MPA-capped water-soluble with strong affinity to TiO₂ due to the coordination of carboxyl and titanium, and the deposition procedure can be accomplished in less than 2 h. In Fig. 2a, the rather deep color (nearly black) of the sensitized film electrodes indicates high surface coverage of QDs on the TiO₂ film, and also, the strong light harvesting capacity of these QDs sensitizers. Fig. 2b shows the TEM images of CISE-ZnS QD sensitized TiO₂ film electrodes. It can be seen that the larger particles (TiO₂, about 20~40 nm) were covered densely with smaller monodispersed spherical particles (CISE-ZnS QDs, 3~4 nm), which imparts vivid evidence of the dense and uniform distribution of the QDs onto TiO₂ mesoporous film. This outstanding QDs coverage and light absorbing capacity pave the way for excellent performance of the resulting cell devices as discussed below.

Compared with other approaches to tether the QDs onto TiO₂ film, for example the *in situ* chemical bath deposition (CBD), successive ionic layer adsorption and reaction (SILAR) or other routes,^{16,43-45} this linker-assisted *ex situ* ligand exchange approach, reveals the advantage of the flexibility to exploit high quality QDs sensitizers, as we successfully employed the alloy configuration of CISE-ZnS QDs to the QDSCs. And also, utilizing small-sized CISE-based QDs with high affinity of short ligand (MPA) resulted in better penetration of QDs into TiO₂ matrix and high coverage of the sensitizers. After this ligand-assisted *ex situ*

assembly approach, we have achieved outstanding photovoltaic performance of the CISE-based cells with the following assembling work, as is supported by the electrochemical measurements.

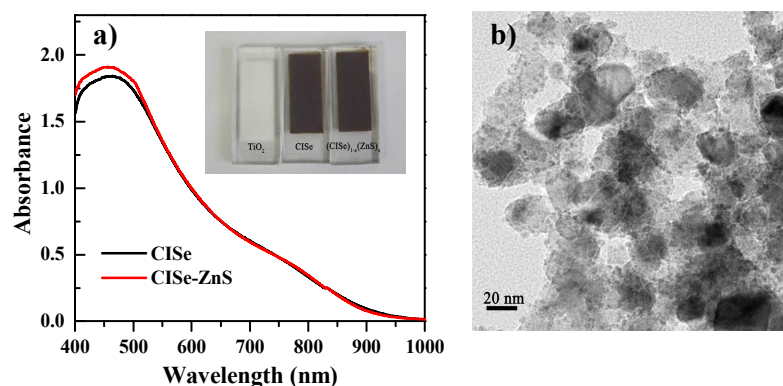


Fig. 2 (a) Diffuse reflectance absorption spectra of CISE (black) and CISE-ZnS QDs (red) deposited on TiO₂ mesoporous film, and inset is the photograph of two QD-sensitized TiO₂ film electrodes compared with the plain TiO₂ film, (b) TEM images of CISE-ZnS QDs (small particles, ~4 nm) sensitized TiO₂ film (large particles, ~20 nm).

Photovoltaic Performance. In the following fabrication procedure, the sensitized film was further passivated by a thin layer of ZnS through the SILAR route, which was confirmed to be a quite effective way to prevent the charge recombination in QDSCs.⁴⁶ After the deposition of the ZnS layers, the QD-sensitized TiO₂ mesoporous film electrode was assembled with Cu₂S counter electrode, where polysulfide electrolyte was fulfilled in between, spaced by a binder clip. To further evaluate the photovoltaic performance of the assembled cell devices, current-voltage characteristics were measured and the J - V curves are shown in Fig. 3a. Photovoltaic parameters (J_{sc} , V_{oc} , FF, and PCE) are extracted from the J - V curves, and the average values of 6 parallel cells together with the values for the champion cell are collected in Table 1. The champion cells of CISE and CISE-ZnS based QDSCs show an efficiency of 6.02% and 6.79%, respectively. These values, as far as we know, are of the highest PCE value in the CISE-based QDSCs and also among the best performances in the whole liquid-junction solar cells.^{25,28} The high efficiency is the result of distinguished light harvesting capacity of the sensitizers and effective loading of the QDs sensitizers, which contributes to boost the J_{sc} to about 22 mA/cm², as is further discussed in the IPCE result. Meanwhile, the design of ZnS alloy configuration QDs structure is of great importance to achieve this high PCE value, which is to reduce the charge recombination both from internal of the QDs and at the interface with the electrolyte. This is obviously reflected on the comparison of the V_{oc} , with the

averaged V_{oc} value of CISE-ZnS based QDSCs increased to 0.584 V (0.03 V more than that of CISE cells), implying the significance of the alloying configuration, in light of the less charge recombination and higher charge extraction efficiency. The wide band gap ZnS constituent in the CISE-ZnS QD sensitizer reduces the defects on the surface of the QDs and shields from charge recombination, resulting in higher PCE values.

Table 1 Photovoltaic Parameters Extracted from $J-V$ Measurements

Cells	J_{sc} (mA/cm ²)	V_{oc} (V)	FF	PCE (%)
CISE ^a	21.42	0.550	0.511	6.02
CISE ^b	21.11	0.548	0.511	5.95±0.07
CISE-ZnS ^a	22.61	0.583	0.515	6.79
CISE-ZnS ^b	22.25	0.584	0.518	6.73±0.06

^a Champion cells; ^b Average value of six parallel cells

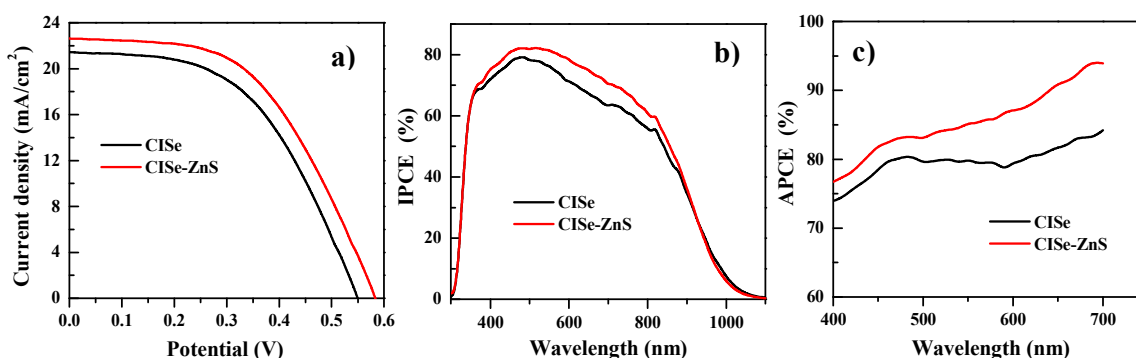


Fig. 3 (a) $J-V$ curves of CISE (black) and CISE-ZnS cells (red) champion cells under the irradiation of 1 full sun, (b) Incident photon to current efficiency (IPCE) curves and (c) absorbed photon-to-electron conversion efficiency (APCE).

The incident photon conversion efficiency (IPCE) or termed as external quantum efficiency (EQE) was investigated for these QDSCs. From the Fig. 3b, a fairly wide response wavelength range of both CISE and CISE-ZnS cells were displayed, with the surprisingly large absorption onset at more than 1000 nm, which is in consistent with the absorption spectra in Fig. 2a. Meanwhile, both the CISE and CISE-ZnS based cells performed relatively high IPCE

values, in which the value of CISE-ZnS based cells peaked at $\sim 80\%$ and was slightly higher than the CISE based ones. It can be deduced that the broad photon response range is the result of narrow bandgap of CISE or CISE-ZnS sensitizers. From the equation: $IPCE = LHE \times \phi_{inj} \times \eta_{cc}$, in which LHE stands for light-harvesting efficiency, ϕ_{inj} for the electron-injection efficiency and η_{cc} for the charge collection efficiency,^{47,48} we can infer that the difference of the IPCE value is due to the better charge collecting or electron-injection performance of the CISE-ZnS cells, since their LHE ($LHE\% = 1 - 10^{-Abs(\lambda)}$) is almost at the same level as indicated by the absorption profile shown in Figure 2a. By calculating the integral of the incident photon flux density and the IPCE value, calculated J_{sc} values for CISE and CISE-ZnS cells (21.02 mA/cm^2 and 22.55 mA/cm^2 , respectively) are similar to their measured J_{sc} listed in Table 1. As another important characteristic of a solar cell, APCE (absorbed photon-to-electron conversion efficiency) is also used to study the conversion of the absorbed photon to current in the external circuit. As is shown in Fig. 3c, in the range of 400 to 700 nm, the CISE-ZnS cells demonstrate a higher APCE value than that of CISE. This reveals that CISE-ZnS cells show better photocurrent conversion efficiency, and from the equation of $APCE = IPCE/LHE = \phi_{inj} \times \eta_{cc}$,^{47,49} the alloy of ZnS with CISE notably improves the performance of the electron collection and/or injection.

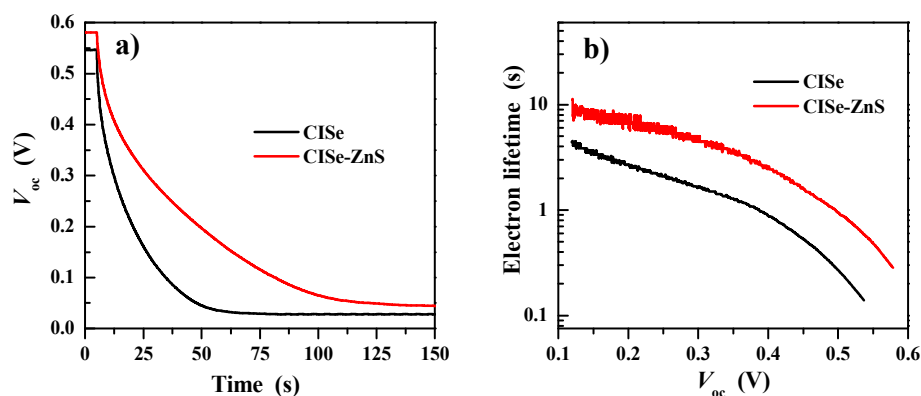


Fig. 4 (a) V_{oc} decay curves of the CISE (black) and CISE-ZnS cells (red) recorded during the relaxation from illuminated quasi-equilibrium to the dark, (b) Electron lifetime derived from OCVD measurements.

Open Circuit Voltage Decay. Open circuit voltage decay (OCVD) analysis was implemented to investigate the different electron recombination processes of these two kind of sensitized solar cells, which is a valid way to calculate the electron lifetime from the open circuit voltage decay information. The measurement procedure is referred to the previous reports.⁵⁰ At the very beginning of measurement, the cells were illuminated by a white LED with intensity of 100 mW cm^{-2} to a steady voltage, then the light is switched off and the open circuit voltage decay information was recorded. From Fig. 4a, it can be observed that the transient V_{oc} values of both cells start stable at their open circuit voltages with the illumination, and continue to decay to nearly 0 V in darkness. Whereas the decay time of these two cells is prominently different. Apparently, the CISE-ZnS cells exhibit much longer decay time than that of the CISE cells. Moreover, the V_{oc} decay rate is a direct reflection of the electron lifetime, since the excess electron undergoes recombination with the trap states and oxidative species in electrolyte when the interruption of illumination occurs. The electron lifetime, τ_n , can be estimated by the equation:

$$\tau_n = -\frac{k_B T}{e} \left(\frac{dV_{oc}}{dt} \right)^{-1}$$

k_B is the Boltzmann constant, T is the absolute temperature, and e is the electronic charge.⁵⁰⁻⁵² From Fig. 4b, we can learn that the calculated electron lifetime (τ_n) of the CISE-ZnS cells is longer than that of CISE cells at the same V_{oc} . This is consistent with the PL results that the PL intensity increased when a certain more amount of ZnS was incorporated into the CIS QDs. Since all devices are treated with a ZnS overlayer by SILAR method to reduce the recombination at the electrode/electrolyte interface,⁵³ we can infer that the slower electron leakage might presumably result from the reduction of the trapping states at the $\text{TiO}_2/\text{CISE-ZnS}$ interface compared to the plain nanocrystals. These data all indicate that the homogeneous or gradient alloy structure of the CISE-ZnS QDs favors the photovoltaic performance of the resulting solar cells in comparison with the plain CISE based QDSCs.

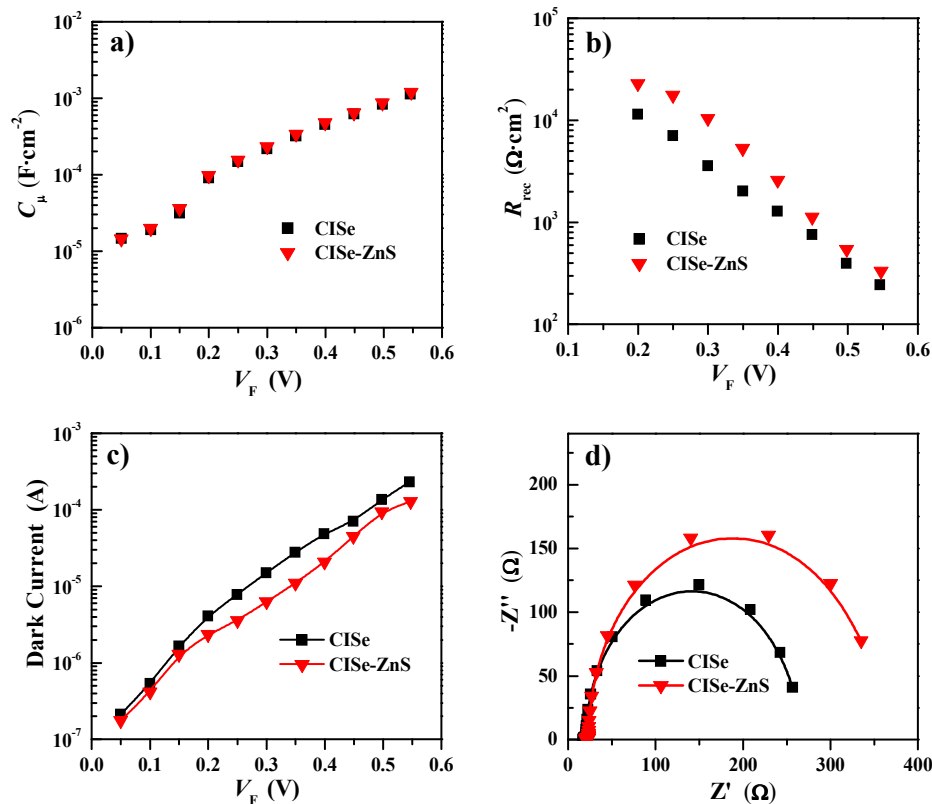


Fig. 5 EIS characterization of the CISE-ZnS cells (red) compared with plain CISE cells (black), (a) chemical capacitance C_μ , (b) recombination resistance R_{rec} , (c) dark current on corrected voltage V_F , and (d) Nyquist plots of both cells at the forward bias of -0.55 V.

Table 2 Simulated Values of Resistance (R) and Capacitance (C) of CISE and CISE-ZnS cells under the Forward Bias of -0.55 V

Cells	R_s ($\Omega \text{ cm}^2$)	C_μ ($mF \text{ cm}^{-2}$)	R_{rec} ($\Omega \text{ cm}^2$)	τ_n (ms)
CISE	17.38	1.13	243.30	274.93
CISE-ZnS	20.46	1.20	331.00	397.20

Impedance Spectroscopy. Charge transport and recombination dynamics in the mesoporous film electrode are investigated by electrochemical impedance spectroscopy (EIS), as is illustrated in the figures of the Nyquist curves. We have recorded the EIS at different forward biases, ranging from 0 V to -0.55 V (near the V_{oc}) under dark conditions. Equivalent

circuit model was built according to our previous work,^{12,25} and the results are presented by using corrected voltage V_F to subtract the effect of the series resistance on the voltage, where $V_F = V_{app} - V_{series}$.⁵⁴ In this equation, V_{app} stands for the applied voltage during the measurement, and V_{series} for voltage drop at series resistance, which is calculated from $V_{series} = [j/(j_{sc} - j)] \int_{j_{sc}}^j R_{series} dj$.⁵⁵ From Fig. 5a, the chemical capacitances (C_{μ}) of sensitized photoelectrode were found similar for both CISE cells and CISE-ZnS cells. As C_{μ} reveals the electron density change under a small potential drop,⁵⁶ we can be informed that the photoelectrodes of the CISE and CISE-ZnS cells shares similar electron density, because the difference of the two sensitizers to influence the conduction band of TiO_2 is not dominant. However, the disparity between the R_{rec} (recombination resistance) of CISE and CISE-ZnS cells is apparent, for CISE-ZnS cells always perform a higher recombination resistance value with the variation of the potential from Fig. 5b. This is evidently indicative of the suppressed electron recombination of the CISE-ZnS cells, mainly due to the configuration of the alloying with ZnS which worked as obstructions against electron recombination in the interface of QDs with electrolyte. The result of the dark current is in well accordance with the R_{rec} result, as is exhibited in Fig. 5c that the value of CISE-ZnS cells is all below that of the CISE cells at the same potential. The information of less generated back electrons also indicates the blocking of the charge recombination. Further comparison of Nyquist plots for CISE and CISE-ZnS cells at the forward bias of -0.55 V are presented in Fig. 5d. The larger semiarc of the CISE-ZnS cells, compared with the one of the CISE cells, suggests that charge transfer resistance between the photoelectrode and the polysulfide electrolyte is much larger. The result of the calculated electron lifetime, τ_n , agrees with the OCVD measurement results, showing that CISE-ZnS cells have lower charge recombination rate between the photoelectrode and the surroundings. With respect to other charge recombination hindering approaches, such as core/shell structure engineered via ion exchange route,^{25,28} the CISE-ZnS alloy structuring in our work, exhibits compelling performance in reducing charge recombination and improving the power conversion efficiency, moreover, this is also a more convenient way of one pot synthesis. All these results confirm that the alloy configuration in CISE-ZnS QDs is an effective route to resist charge recombination, more importantly, with the intrinsic properties of the QDs, it eventually contributes to the achievement of excellent photovoltaic performance.

4. Conclusions

In summary, a kind of high efficiency “green” CISE-based QDSC has been successfully developed. The intrinsic NIR absorbing properties of CISE and CISE-ZnS alloyed QDs make them ideal candidate in fabricating a photovoltaic device, and more interestingly, suppressed charge recombination and concomitant better photovoltaic performance were obtained in the CISE-ZnS QD based QDSCs. This demonstrates the outstanding architecture of the obtained CISE-ZnS alloy QDs in serving as light-harvesting sensitizer material in QDSC. The retarded charge recombination process was revealed by OCVD measurement and impedance spectroscopy. Benefiting from the effective linker-assisted *ex situ* ligand exchange approach to achieve high loading of the QDs onto TiO₂ photoanode, and the promising alloy configuration, these CISE-ZnS based QDSCs showed excellent photovoltaic properties with an efficiency of 6.79 %, which is among the best performances for liquid-junction QDSCs and also demonstrates the comparable photovoltaic performance for the “green” CISE QDs sensitizing materials to the toxic cadmium and lead chalcogenide QD materials.

Acknowledgements

We acknowledge the National Natural Science Foundation of China (No. 21175043), the Science and Technology Commission of Shanghai Municipality (11JC1403100, 12ZR1407700), and the Fundamental Research Funds for the Central Universities for financial supports.

References

- 1 I. J. Kramer and E. H. Sargent, *Chem. Rev.*, 2014, **114**, 863-882.
- 2 Y. Bai, I. Mora-Seró, F. De Angelis, J. Bisquert and P. Wang, *Chem. Rev.*, 2014, **114**, 10095-10130.
- 3 M. He, D. Zheng, M. Wang, C. Lin and Z. Lin, *J. Mater. Chem. A*, 2014, **2**, 5994-6003.
- 4 I. Hod and A. Zaban, *Langmuir*, 2014, **30**, 7264-7273.
- 5 X. Lan, S. Masala and E. H. Sargent, *Nat. Mater.*, 2014, **13**, 233-240.
- 6 O. E. Semonin, J. M. Luther, S. Choi, H. Y. Chen, J. Gao, A. J. Nozik and M. C. Beard, *Science*, 2011, **334**, 1530-1533.
- 7 P. V. Kamat, *J. Phys. Chem. C*, 2008, **112**, 18737-18753.
- 8 D. R. Baker and P. V. Kamat, *Adv. Funct. Mater.*, 2009, **19**, 805-811.
- 9 V. González-Pedro, C. Sima, G. Marzari, P. P. Boix, S. Giménez, Q. Shen, T. Dittrich and I. Mora-Seró, *Phys. Chem. Chem. Phys.*, 2013, **15**, 13835-13843.
- 10 H. Lee, M. Wang, P. Chen, D. R. Gamelin, S. M. Zakeeruddin, M. Grätzel and M. K. Nazeeruddin, *Nano Lett.*, 2009, **9**, 4221-4227.
- 11 W. Ma, J. M. Luther, H. Zheng, Y. Wu and A. P. Alivisatos, *Nano Lett.*, 2009, **9**, 1699-1703.
- 12 J. Wang, I. Mora-Seró, Z. Pan, K. Zhao, H. Zhang, Y. Feng, G. Yang, X. Zhong and J. Bisquert, *J. Am. Chem. Soc.*, 2013, **135**, 15913-15922.
- 13 P. K. Santra and P. V. Kamat, *J. Am. Chem. Soc.*, 2012, **134**, 2508-2511.
- 14 H. Zhang, K. Cheng, Y. M. Hou, Z. Fang, Z. X. Pan, W. J. Wu, J. L. Hua and X. H. Zhong, *Chem. Commun.*, 2012, **48**, 11235-11237.
- 15 P. M. Allen and M. G. Bawendi, *J. Am. Chem. Soc.*, 2008, **130**, 9240-9241.
- 16 M. Booth, A. P. Brown, S. D. Evans and K. Critchley, *Chem. Mater.*, 2012, **24**, 2064-2070.
- 17 M. Wang, S. K. Batabyal, Z. Li, D. Li, S. G. Mhaisalkar and Y. M. Lam, *RSC Adv.*, 2013, **3**, 9829-9834.
- 18 D. Aldakov, A. Lefrançois and P. Reiss, *J. Mater. Chem. C*, 2013, **1**, 3756-3776.
- 19 J. Y. Chang, J. M. Lin, L. F. Su and C. F. Chang, *ACS Appl. Mater. Interfaces*, 2013, **5**, 8740-8752.
- 20 J. Y. Chang, L. F. Su, C. H. Li, C. C. Chang and J. M. Lin, *Chem. Commun.*, 2012, **48**, 4848-4850.
- 21 T. L. Li, Y. L. Lee and H. Teng, *Energy Environ. Sci.*, 2012, **5**, 5315-5324.
- 22 J. Luo, H. Wei, Q. Huang, X. Hu, H. Zhao, R. Yu, D. Li, Y. Luo and Q. Meng, *Chem. Commun.*, 2013, **49**, 3881-3883.
- 23 P. K. Santra, P. V. Nair, K. George Thomas and P. V. Kamat, *J. Phys. Chem. Lett.*, 2013, **4**, 722-729.
- 24 G. P. Xu, S. L. Ji, C. H. Miao, G. D. Liu and C. H. Ye, *J. Mater. Chem.*, 2012, **22**, 4890-4896.
- 25 Z. Pan, I. Mora-Seró, Q. Shen, H. Zhang, Y. Li, K. Zhao, J. Wang, X. Zhong and J. Bisquert, *J. Am. Chem. Soc.*, 2014, **136**, 9203-9210.
- 26 J. A. M. AbuShama, S. Johnston, T. Moriarty, G. Teeter, K. Ramanathan and R. Noufi, *Prog.*

- Photovolt: Res. Appl.*, 2004, **12**, 39-45.
- 27 E. Witt and J. Kolny-Olesiak, *Chem. Eur. J.*, 2013, **19**, 9746-9753.
- 28 H. McDaniel, N. Fuke, N. S. Makarov, J. M. Pietryga and V. I. Klimov, *Nat. Commun.*, 2013, **4**, 2887.
- 29 H. McDaniel, N. Fuke, J. M. Pietryga and V. I. Klimov, *J. Phys. Chem. Lett.*, 2013, **4**, 355-361.
- 30 C.-F. Du, T. You, L. Jiang, S.-Q. Yang, K. Zou, K.-L. Han and W.-Q. Deng, *RSC Adv.*, 2014, **4**, 33855-33860.
- 31 S. Kim, M. Kang, S. Kim, J. H. Heo, J. H. Noh, S. H. Im, S. I. Seok and S. W. Kim, *ACS nano*, 2013, **7**, 4756-4763.
- 32 M. G. Panthani, V. Akhavan, B. Goodfellow, J. P. Schmidtke, L. Dunn, A. Dodabalapur, P. F. Barbara and B. A. Korgel, *J. Am. Chem. Soc.*, 2008, **130**, 16770-16777.
- 33 M. Wang, S. K. Batabyal, Z. Li, D. Li, S. G. Mhaisalkar and Y. M. Lam, *RSC Adv.*, 2013, **3**, 9829-9834.
- 34 J. Yang, J. Y. Kim, J. H. Yu, T. Y. Ahn, H. Lee, T. S. Choi, Y. W. Kim, J. Joo, M. J. Ko and T. Hyeon, *Phys. Chem. Chem. Phys.*, 2013, **15**, 20517-20525.
- 35 M. G. Panthani, C. J. Stolle, D. K. Reid, D. J. Rhee, T. B. Harvey, V. A. Akhavan, Y. Yu and B. A. Korgel, *J. Phys. Chem. Lett.*, 2013, **4**, 2030-2034.
- 36 H. Z. Zhong, Z. B. Wang, E. Bovero, Z. H. Lu, F. C. J. M. van Veggel and G. D. Scholes, *J. Phys. Chem. C*, 2011, **115**, 12396-12402.
- 37 S. Li, Z. Zhao, Q. Liu, L. Huang, G. Wang, D. Pan, H. Zhang and X. He, *Inorg. Chem.*, 2011, **50**, 11958-11964.
- 38 J. B. Sambur, and B. A. Parkinson, *J. Am. Chem. Soc.*, 2010, **132**, 2130-2131.
- 39 N. Guijarro, E. Guillén, T. Lana-Villarreal and R. Gómez, *Phys. Chem. Chem. Phys.*, 2014, **16**, 9115-9122.
- 40 Z. Pan, K. Zhao, J. Wang, H. Zhang, Y. Feng and X. Zhong, *ACS nano*, 2013, **7**, 5215-5222.
- 41 Z. Du, H. Zhang, H. Bao and X. Zhong, *J. Mater. Chem. A*, 2014, **2**, 13033-13040.
- 42 L. Liu, X. Guo, Y. Li and X. Zhong, *Inorg. Chem.*, 2010, **49**, 3768-3775.
- 43 D. F. Watson, *J. Phys. Chem. Lett.*, 2010, **1**, 2299-2309.
- 44 O. Niitsoo, S. K. Sarkar, C. Pejoux, S. Rühle, D. Cahen and G. Hodes, *Photochem. Photobio. A: Chem*, 2006, **181**, 306-313.
- 45 D. R. Baker and P. V. Kamat, *Adv. Funct. Mater.*, 2009, **19**, 805-811.
- 46 E. M. Barea, M. Shalom, S. Giménez, I. Hod, I. Mora-Seró, A. Zaban and J. Bisquert, *J. Am. Chem. Soc.* 2010, **132**, 6834-6839.
- 47 Z. Yang, C. Y. Chen, P. Roy and H. T. Chang, *Chem. Commun.*, 2011, **47**, 9561-9571.
- 48 N. Fuke, L. B. Hoch, A. Y. Kuposov, V. W. Manner, D. J. Werder, A. Fukui, N. Koide, H. Katayama and M. Sykora, *ACS nano*, 2010, **4**, 6377-6386.
- 49 M. K. Nazeeruddin, A. Kay, I. Rodicio, R. Humphry-Baker, E. Mueller, P. Liska, N. Vlachopoulos and M. Grätzel, *J. Am. Chem. Soc.*, 1993, **115**, 6382-6390.

- 50 Q. Zhang, X. Guo, X. Huang, S. Huang, D. Li, Y. Luo, Q. Shen, T. Toyoda and Q. Meng, *Phys. Chem. Chem. Phys.*, 2011, **13**, 4659-4667.
- 51 J. Bisquert, A. Zaban, M. Greenshtein and I. Mora-Seró, *J. Am. Chem. Soc.*, 2004, **126**, 13550-13559.
- 52 V. González-Pedro, X. Xu, I. Mora-Seró and J. Bisquert, *ACS nano*, 2010, **4**, 5783-5790.
- 53 N. Guijarro, J. M. Campiñ, Q. Shen, T. Toyoda, T. Lana-Villarreal and R. Gómez, *Phys. Chem. Chem. Phys.*, 2011, **13**, 12024-12032.
- 54 F. Fabregat-Santiago, J. Bisquert, E. Palomares, L. Otero, D. Kuang, S. M. Zakeeruddin, and M. Grätzel, *J. Phys. Chem. C*, 2007, **111**, 6550-6560.
- 55 F. Fabregat-Santiago, G. Garcia-Belmonte, I. Mora-Seró and J. Bisquert, *Phys. Chem. Chem. Phys.*, 2011, **13**, 9083-9118.
- 56 V. González-Pedro, X. Xu, I. Mora-Seró and J. Bisquert, *ACS nano*, 2010, **4**, 5783-5790.

The table of contents

CuInSe₂ and CuInSe₂-ZnS based High Efficiency “Green” Quantum Dot Sensitized Solar Cells

Wenjie Li, Zhenxiao Pan, and Xinhua Zhong*

The CISE-based QDs with ZnS alloy configuration exhibit higher superior optoelectronic properties and chemical stability, and thus, the fabrication of CISE-ZnS QDSCs shows better photovoltaic performance.

